Epitaxial single-layer NbS_2 on Au(111): Synthesis, structure, and electronic properties

Raluca-Maria Stan,[1] Sanjoy K. Mahatha,[1] Marco Bianchi,[1] Charlotte E. Sanders,[2] Davide Curcio,[1] Philip Hofmann,[1,*] and Jill A. Miwa[1,†]

[1]*Department of Physics and Astronomy, Interdisciplinary Nanoscience Center (iNANO), Aarhus University, 8000 Aarhus C, Denmark*
[2]*Central Laser Facility, STFC Rutherford Appleton Laboratory, Harwell OX11 0QX, United Kingdom*

(Received 11 January 2019; published 23 April 2019)

We report on the epitaxial growth of single-layer NbS_2 on Au(111) and determine both its crystalline and electronic structure by a combination of low-energy electron diffraction, scanning tunneling microscopy, and angle-resolved photoemission spectroscopy. The layer is found to grow in the 1H structural phase with a lattice constant of (3.29 ± 0.03) Å, a value comparable to the bulk 2H NbS_2 lattice constant. The photoemission data reveals a metallic band structure down to a temperature of 30 K. The observed bands are rather broad and consistent with either a strong NbS_2-substrate interaction or with the recently reported interplay of strong many body effects in single-layer NbS_2 [van Loon *et al.*, npj Quantum Mater. **3**, 32 (2018)]. No indications of a charge density wave are observed.

DOI: 10.1103/PhysRevMaterials.3.044003

I. INTRODUCTION

Metallic transition metal dichalcogenides (TMDCs) have been studied for decades due to their susceptibility to many fascinating quantum states, such as charge and spin ordering, Mott insulating states, and superconductivity, and because, more generally, they provide a platform for the study of many-body interactions in nearly two-dimensional (2D) materials [1–3]. The ability to isolate single-layer (SL) TMDCs [4–6] now extends these types of investigations to genuinely 2D systems. This avenue of research is rather compelling, especially since it has turned out that the assumption of a purely 2D character in van der Waals bonded bulk compounds may not be generally valid, after all [7,8]. Moreover, the properties of SL materials may be tuned by the choice of substrate, as this interaction can have a significant impact on the electronic properties of the 2D material, for instance, by screening the otherwise strongly enhanced Coulomb interaction [9–12]. Studies of metallic SL TMDCs are considerably more challenging than of their semiconducting counterparts, such as MoS_2, due to their strongly enhanced chemical reactivity, which may also be responsible for the partly contradictory results on, for example, the superconducting transition temperature in atomically thin 2H TaS_2 [13–15] or the charge density wave (CDW) transition temperature in SL $NbSe_2$ [16,17].

The isoelectronic sulphides and selenides of vandium, niobium, and tantalum show an intriguing competition between magnetism, charge density waves, and Mott insulating behavior. It is not unusual for several of these quantum states to be observed in the same material at different temperatures or even simultaneously. 2H NbS_2 stands out in this class of materials because it is widely considered to be the only case for which superconductivity can be observed ($T_c \approx 6$ K) in the absence of charge density wave states [18–20] (even though this long-held point of view has recently been called into question [21]).

While few layer (3R) [22] and even single-layer NbS_2 [23] have been successfully synthesized, little is known about the different ground states in SL NbS_2. Density functional theory and GW calculations predict SL NbS_2 to be metallic with a half-filled upper valence band that is well separated from other electronic states [24,25]. In this approximation, the ground state of the system is not magnetic but it is close to magnetic phases [26,27]. Very recently, the electronic structure of SL NbS_2 was studied with the inclusion of several types of many-body effects, such as short- and long-range Coulomb interactions and electron-phonon interactions [28]. The study found that each of these interactions has a significant effect on the spectral function, leading to situations that are drastically different from the bare single particle dispersion. Rather unexpectedly, the combined effect of the many-body interactions restores the spectral function to what essentially resembles a broadened version of the bare dispersion. From these results, SL NbS_2 might be expected to be a unique case for experimentally tuning different many-body interactions by, for example, the choice of doping or substrate, in order to reach a multitude of desired ground states.

In this article, we report on the synthesis of SL NbS_2 on Au(111). Due to the epitaxial character of the system, the growth is restricted to a single orientation (and its mirror domain), thereby allowing both the crystalline and electronic structure of the SL NbS_2 to be probed with spatially averaging techniques such as low-energy electron diffraction (LEED) and angle-resolved photoemission spectroscopy (ARPES). Consistent with a strong NbS_2-Au(111) interaction, or with an interplay of strong many-body effects in the SL NbS_2 [28], or with a combination of both, the ARPES data divulges a metallic band structure with broad bands.

*philip@phys.au.dk
†miwa@phys.au.dk

II. EXPERIMENT

The growth of epitaxial SL NbS_2 on Au(111) was based on a growth technique previously developed for other SL TMDCs [29–34], with the transition metal being evaporated onto a single crystal in a sulfur-rich atmosphere. Initially the Au(111) substrate (Mateck) was cleaned by repeated cycles of ion bombardment (Ne^+ at 1.5 keV) and annealing to 650 °C under ultrahigh vacuum (UHV) conditions. The surface order and cleanliness were established by scanning tunneling microscopy (STM); the substrate was sputtered and annealed until STM revealed an atomically clean surface with the characteristic herringbone reconstruction [35]. Niobium was evaporated from an electron beam evaporator (Nb rod of 99.9% purity from Goodfellow) onto the clean Au(111) surface, held at room temperature, in a pressure of 2×10^{-6} mbar of dimethyl disulphide (DMDS, $C_2H_6S_2$, with >99% purity from Sigma-Aldrich). The sample was subsequently annealed for 30 min at ≈450 °C, while the same pressure of DMDS was maintained. Finally, the DMDS was pumped out of the chamber and the sample was annealed to ≈600 °C for 30 min in order to eliminate residual physisorbed DMDS, and to improve the overall crystalline quality of the SL NbS_2.

Synthesis and STM characterization of the SL NbS_2 growth were performed in a dedicated growth chamber (base pressure of 10^{-10} mbar) using a homebuilt Aarhus-type STM [36]. Tips were made from a Pt-Ir alloy. All STM images were processed using free WSxM software [37] and generally involved plane flattening and calibrating to reflect the known atomic lattice parameter of the clean Au(111) surface. The uncertainties associated with the quoted lengths determined by STM arise mainly from thermal drift and/or piezocreep. LEED and ARPES measurements were performed at the SGM3 beamline at the ASTRID2 synchrotron radiation facility [38]. ARPES and LEED data were collected at 30 K. All ARPES measurements presented here were performed with a photon energy of 50 eV with an energy and angular resolution better than 65 meV and 0.2°, respectively.

To transfer the reactive SL NbS_2, in air, from the growth/STM chamber to the ARPES/LEED chamber, the sample was protected by a DMDS capping layer. The capping layer was prepared by keeping the grown SL NbS_2 sample at room temperature in a DMDS pressure of 2×10^{-6} mbar for 30 min. Once the sample was reintroduced to UHV conditions at the SGM3 beamline, it was annealed to ≈600 °C for 30 min to remove the physisorbed capping layer. STM images were acquired after the removal of the capping layer in the ARPES chamber (not shown), and were consistent with a surface cleanliness on par with SL NbS_2 samples grown without a capping layer.

III. RESULTS AND DISCUSSION

Figure 1(a) shows the topography of SL NbS_2 on Au(111) measured by STM. Several domains of SL NbS_2 are visible with smaller regions of clean Au in between. Although not visible in the STM image presented here, the dark regions between the SL NbS_2 domains are identified as clean Au because either Au atoms and/or a typically distorted herringbone structure are observed [39]. The SL NbS_2 domains cover approximately 75% of the surface, and are irregular in shape with sharp boundaries between adjacent domains. A well-ordered hexagonal moiré is visible, due to the different periodicity of the substrate and the epitaxial layer. The periodicity of the moiré is 20.7 Å, as determined from Fourier transform analysis of the STM data. The moiré pattern is qualitatively very similar to that observed for other epitaxial SL TMDCs on Au(111), particularly MoS_2, WS_2, and TaS_2 [32,33,39], and the minor distortions in the regularity of the moiré, especially close to edges and domain boundaries, can be understood in terms of local strain in the material [40].

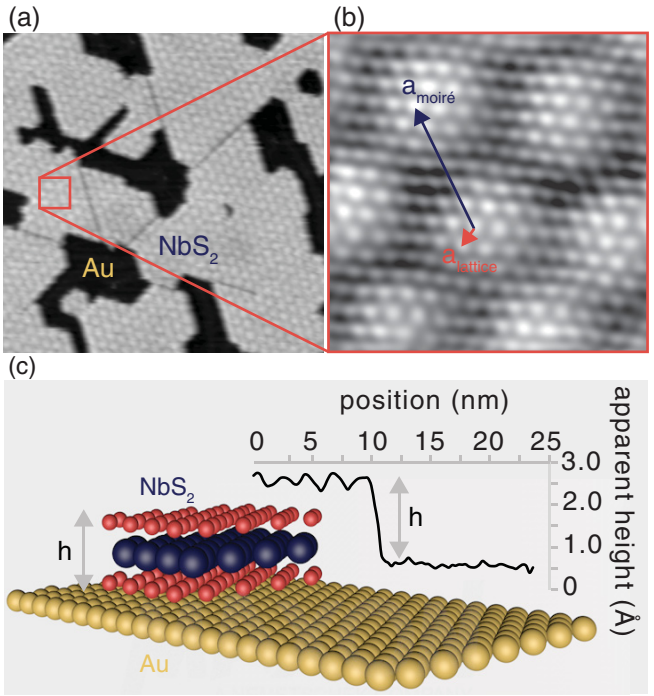

FIG. 1. STM characterization of SL NbS_2 on Au(111). (a) A (621 × 621) Å^2 overview revealing irregularly shaped domains and a hexagonal moiré pattern. Image parameters: $I_t = 0.46$ nA; $V_b = -0.86$ V. (b) A (50 × 50) Å^2 atomically resolved STM image of the SL NbS_2. The smaller hexagonal atomic structure and the larger hexagonal moiré pattern are both visible in the image. Image parameters: $I_t = 1.68$ nA; $V_b = -0.31$ V. (c) A schematic of the SL NbS_2 (sulfur atoms are indicated by red spheres and the niobium by blue ones) on a Au substrate, with the height of the single layer indicated by "h". A line profile taken across the edge of a NbS_2 domain with the corresponding measured apparent height demarcated by the double headed gray arrow. The apparent height was measured to be (3.1 ± 0.2) Å.

Figure 1(b) shows an atomically resolved image from which a hexagonal lattice constant of (3.4 ± 0.3) Å was extracted. This value is in agreement with the bulk lattice parameter of 3.3 Å for 2H (trigonal prismatic) NbS_2 [1]. It is not straightforward, on the basis of atomically resolved STM images alone, to distinguish between the possible polymorphs of the SL structure, which are either 1H or 1T (octahedral), since both polymorphs possess a hexagonal structure with presumably similar lattice constants.

Figure 1(c) shows a line profile taken across the edge of a domain boundary. The profile reveals an apparent height

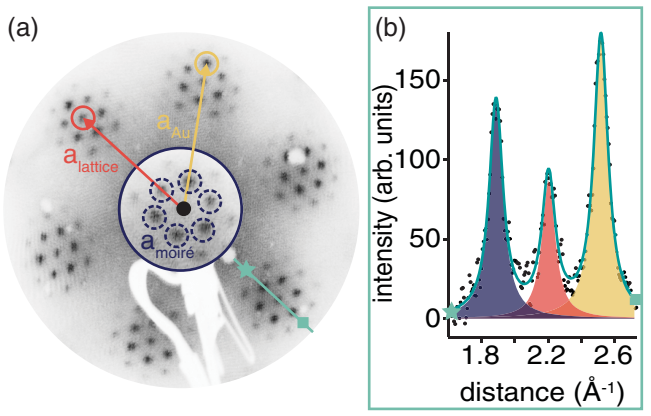

FIG. 2. (a) LEED pattern for SL NbS_2 on Au(111) acquired at 30 K using an electron kinetic energy of 100 eV. The Au (yellow) and SL NbS_2 (red) reciprocal lattice vectors are shown. The LEED reveals six first-order spots in a hexagonal arrangement, and surrounding each of these individual spots are six intense satellite spots, also in a hexagonal arrangement. The inset at the center of the LEED image is a magnified area around a first order spot. The satellite spots arise from the moiré and are marked by the blue dashed lines. (b) A line profile taken through the LEED image along the green line from the star marker to the square marker is presented. The intensity can be well described by three Lorentzian peaks, and the lattice parameter for SL NbS_2 was determined from the peak positions to be (3.29 ± 0.03) Å. The fitting contributions are color-coded according to the designation used for the LEED spots: SL NbS_2 (red), Au (yellow), and moiré (blue).

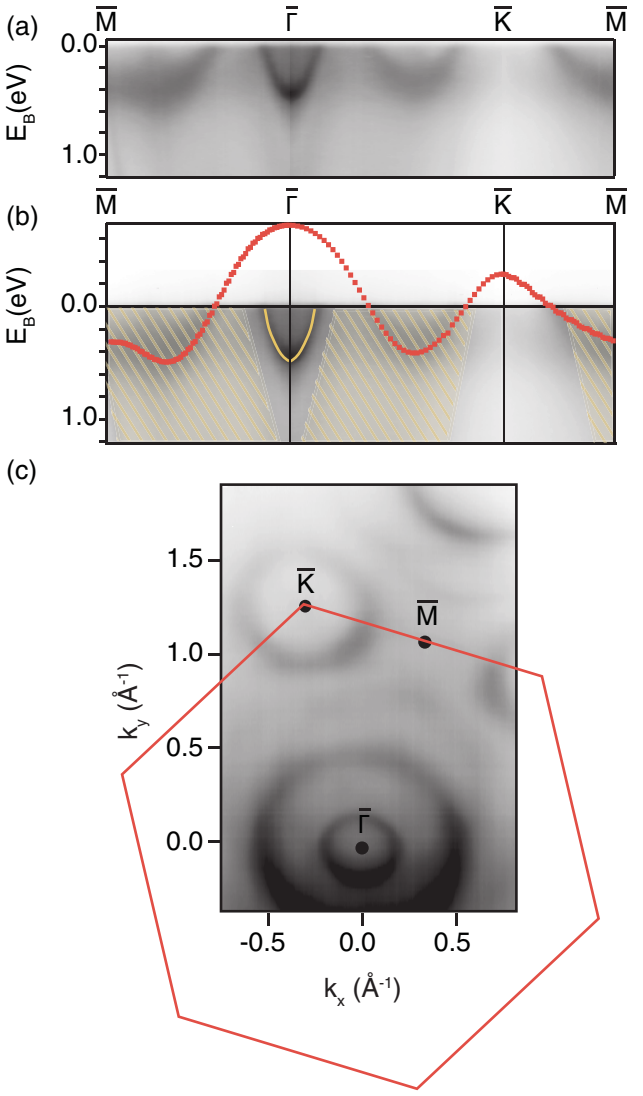

FIG. 3. Photoemission intensity for SL NbS_2 on Au(111). (a) Photoemission intensity along the high symmetry lines of the NbS_2 2D Brillouin zone acquired with a photon energy of 50 eV. (b) The same ARPES data depicted in panel (a) but with the relevant features of the measured band structure marked: the Au surface state is highlighted by the yellow line; the projected bulk bands of the Au are demarcated by the yellow striped and shaded region; the calculated band structure for SL NbS_2 reported by van Loon *et al.* [28] is shown in red. (c) Photoemission intensity at the Fermi energy with $\bar{K}$, $\bar{M}$, and $\bar{\Gamma}$, indicated along with the NbS_2 2D Brillouin zone overlaid in red.

difference of (3.1 ± 0.2) Å between the top of the NbS_2 layer and the Au(111) surface. This value is consistent with the results for similar systems [32,33,39].

The overall ordering on the surface can be studied by LEED. Figure 2(a) shows a LEED pattern revealing the integer order diffraction spots of both the NbS_2 (red circle) and the Au(111) lattice (yellow circle) and the additional spots due to the moiré (dashed blue circle). The two main lattices are well aligned and only one orientation of the SL NbS_2 is observed, albeit with the possibility of mirror domains [41]. An accurate determination of the SL NbS_2 lattice parameter can be achieved by fitting the peak positions in a line cut through the image, as shown in Fig. 2(b). The cut was taken along the green line from the star to the square. The known 2.88 Å lattice parameter of Au(111) was used as a calibration and, from the analyses of this and similar cuts in the corresponding directions, the lattice parameter of SL NbS_2 was determined to be (3.29 ± 0.03) Å, in agreement with the STM results. We note that we do not observe any additional spots in the LEED that could hint at the existence of a charge density wave in SL NbS_2 at 30 K.

Finally, we determine the electronic structure of SL NbS_2 using ARPES. The photoemission intensity along the high symmetry directions of the NbS_2 2D Brillouin zone, acquired with 50 eV photons, is shown in Fig. 3(a). The same data is reproduced in Fig. 3(b) but with salient features marked. Some features crossing the Fermi level can be assigned to the well-known Au(111) surface state around $\bar{\Gamma}$ [42] and the *sp*-bulk band of Au (very weak). The presence of the surface state is ascribed to the remaining clean areas on the surface. The other visible features stem from SL NbS_2: a hole pocket around $\bar{\Gamma}$ and a second hole pocket around $\bar{K}(\bar{K}')$. The parabolic Au(111) surface state is marked by the yellow line. The yellow striped and shaded region indicates the projected bulk bands of Au(111). Overlaid on the data, in red, is the calculated bare dispersion for SL NbS_2 recently reported in Ref. [28]. From this ARPES data, we conclude that SL NbS_2 is metallic and that the general shape of the band structure is consistent with that expected for the 1H polytype [24,25]. The

band structure is essentially the same as observed for SL TaS_2 but without the strong spin-orbit splitting [33].

The calculated band structure has been rigidly shifted by 0.15 eV to higher binding energies in order to attain an approximate agreement between measurement and calculation; however, there is no rigid shift of the calculated band structure that can provide complete agreement with the measured data. Perhaps the lack of quantitative agreement is not entirely surprising, as almost the entire observed band structure falls within the projected bulk bands of Au(111) [43] and therefore some hybridization with the substrate is expected to occur [44–46]. On the other hand, in the very similar case of SL TaS_2 on Au(111), a rigid energy shift can generate excellent agreement between observed bands and calculation for a theoretical free-standing layer [33]. Lastly, we note that there are no indications of gap openings or backfolding of bands in Fig. 3(a), as might be expected in the presence of a CDW.

The photoemission intensity at the Fermi energy is shown in Fig. 3(c) with the high symmetry points indicated and the NbS_2 2D Brillouin zone superimposed on the ARPES data in red. From the size of the Fermi contour, the electron filling of the SL NbS_2 valence band can be estimated. Using the same approach as in Ref. [33], we determine that the upper valence band of SL NbS_2 on Au(111) is filled by (1.36 ± 0.02) electrons per unit cell instead of the expected one electron. This corresponds to an electron concentration of $(1.26 \pm 0.02) \times 10^{15}$ cm^{-2}. Such strong doping effects have also been observed for SL TaS_2 on Au(111) [33]. In that case, they are not necessarily caused by true doping of the SL material and can rather be explained by the hybridization between substrate and SL material, which can lead to band structure modifications reminiscent of doping but without involving actual charge transfer. This "pseudodoping" effect is discussed in detail in Ref. [46]. This is also likely to be the case here.

Despite the excellent crystalline quality revealed by STM and LEED, the SL NbS_2-related features observed in ARPES are very broad compared to those previously observed in other high-quality SL TMDCs. One possible reason for this is the hybridization between SL and substrate states [44,45]. Indeed, past studies of semiconducting SL TMDCs on Au(111) and Ag(111) have found the bands to be sharp only in the spectral region that falls in the projected band gap of the substrate, around the valence band maximum at $\bar{K}$ [47,48]. Here, the SL NbS_2 valence band maximum at $\bar{K}$ is above the Fermi energy, and almost the entire observed band structure falls in the continuum of the Au bulk states, which makes them presumably prone to hybridization. Another possible explanation for the broad bands is the many-body interactions discussed in Ref. [28] that lead to a substantial broadening of the spectral function for the free-standing material.

Detailed analysis of the SL NbS_2 dispersion and linewidth is presented in Fig. 4. Energy distribution curves (EDCs) along the $\bar{\Gamma} - \bar{K}$ direction are shown in Fig. 4(a), and the plotted data correspond to the right hand side of the $\bar{\Gamma}$ point in Fig. 3(a). At high binding energy, the EDCs can be well fitted by a Lorentzian line on a linear background multiplied by a Fermi-Dirac distribution. When the peak approaches the Fermi level, these fits do not produce a satisfactory result. This

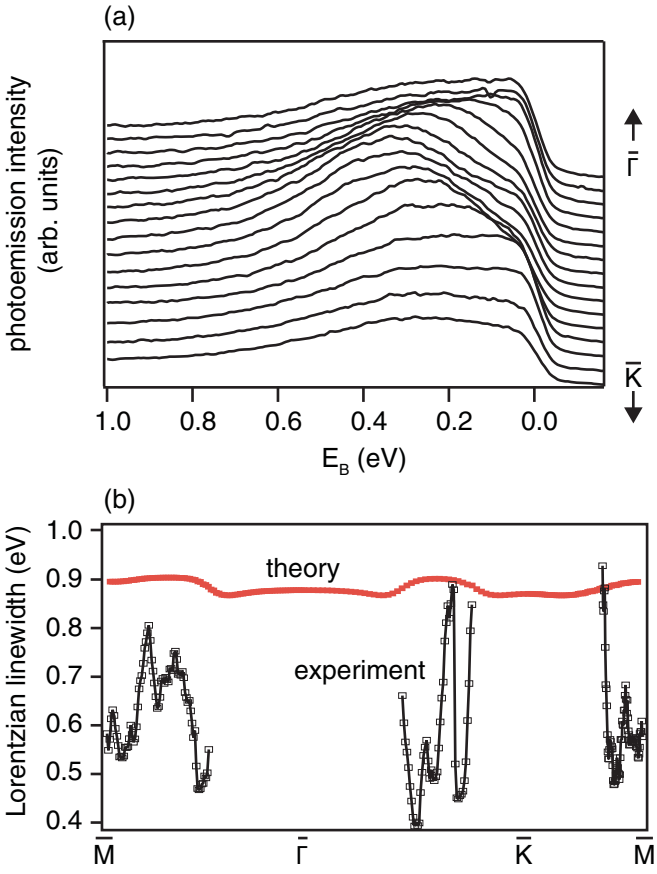

FIG. 4. (a) Data from Fig. 3(a) between $\bar{\Gamma}$ and $\bar{K}$ represented as EDCs. The k step between the curves is ≈0.05 Å. (b) Lorentzian full width at half maximum of the peak in the data of Fig. 3(a) (open markers) along with the corresponding linewidth extracted from the data in Fig. 2(a) of Ref. [28] (filled red markers).

is caused partly by a weak kinklike structure in the dispersion close to the Fermi energy, indicative of strong many-body effects [49,50]. Figure 4(b) shows the resulting Lorentzian linewidth from the fits, together with the Lorentzian linewidth of the corresponding states in the calculated spectral function, including all many-body effects (i.e., $U + V + \lambda$), in Fig. 2(a) of Ref. [28]. The experimental and theoretical linewidths are similar but, interestingly, the experimental values are mostly somewhat smaller, despite the simultaneous presence of many-body interactions and the SL NbS_2-substrate interaction. The experimental linewidth also varies rather irregularly in a small k range. This variation is attributed to the background intensity from Au bands. This effect is most clearly seen in the $\bar{M} - \bar{\Gamma}$ direction, in Fig. 3(a), where a weak Au sp band intersects the dispersion of the NbS_2 band. Note that an EDC linewidth (or the corresponding cut through a calculated spectral function) is not directly proportional to the imaginary part of the electronic self-energy because the slope of the band needs to be taken into consideration as well [50]. Note also that considerably narrower EDCs can be obtained from similar materials (e.g., a Lorentzian width less than 50 meV having been observed for SL WS_2) when many-body interactions are weak and the states fall into the projected bulk band structure of Au(111) [47].

It is difficult to draw detailed conclusions from the comparison of measured and theoretical linewidths without further calculations involving not only the free-standing layer but also the substrate effects. In particular, it would be incorrect to conclude that the calculations overestimate the many-body effects because the calculated linewidth exceeds the measured one. In fact, while the substrate interaction might give rise to an additional broadening of the states via hybridization, the increased screening has the potential to reduce long-range Coulomb interactions in the materials and thereby substantially modify the many-body interaction.

It is possible to compare the resulting dispersion to that of bulk NbS_2 even though there are only very few published ARPES results from that material [51]. The most significant difference is pronounced bilayer splitting (from the two layers in the 2H unit cell) in the uppermost valence band of the bulk crystal. For MoS_2 and WS_2, this bilayer splitting is confined to a narrow region of k space close to $\bar{\Gamma}$ but for NbS_2 it is seen almost throughout the entire band [24]. The bilayer splitting is also clearly detectable in ARPES experiments from bulk NbS_2 [51]. However, as one would expect, it is absent in the data presented here.

IV. CONCLUSIONS

In summary, we have reported the epitaxial growth of SL NbS_2 on Au(111). Excellent structural quality can be realized, as revealed by STM and LEED. The resulting band structure is consistent with a 1H crystalline structure. It reveals strong electron doping that could partly be due to hybridization with the substrate, as previously reported for SL TaS_2 [33,46]. In contrast to the occupied band structure of SL TaS_2 on Au(111), however, clear deviations between the measured band structure and the rigidly shifted calculated bands for a free-standing layer are seen. Finally, the observed spectral features are rather broad. This could also be due to hybridization or to the predicted strong many-body interactions in this system [28]. This could perhaps be investigated further by transferring the growth procedure described here to a more inert substrate or, possibly, by intercalation-induced decoupling of the SL NbS_2 layer from the substrate [48].

ACKNOWLEDGMENTS

We thank the authors of Ref. [28] for helpful discussions and for making their data available to us. This work was supported by the Danish Council for Independent Research, Natural Sciences under the Sapere Aude program (Grants No. DFF-4002-00029 and No. DFF-6108-00409) and by VILLUM FONDEN via the Centre of Excellence for Dirac Materials (Grant No. 11744) and the Aarhus University Research Foundation. Affiliation with the Center for Integrated Materials Research (iMAT) at Aarhus University is gratefully acknowledged.

[1] J. Wilson and A. Yoffe, Adv. Phys. **18**, 193 (1969).
[2] J. Wilson, F. Di Salvo, and S. Mahajan, Adv. Phys. **24**, 117 (1975).
[3] K. Rossnagel, J. Phys.: Condens. Matter **23**, 213001 (2011).
[4] K. F. Mak, C. Lee, J. Hone, J. Shan, and T. F. Heinz, Phys. Rev. Lett. **105**, 136805 (2010).
[5] K. S. Novoselov, D. Jiang, F. Schedin, T. J. Booth, V. V. Khotkevich, S. V. Morozov, and A. K. Geim, Proc. Natl. Acad. Sci. USA **102**, 10451 (2005).
[6] A. Splendiani, L. Sun, Y. Zhang, T. Li, J. Kim, C.-Y. Chim, G. Galli, and F. Wang, Nano Lett. **10**, 1271 (2010).
[7] D. Di Sante, P. K. Das, C. Bigi, Z. Ergönenc, N. Gürtler, J. A. Krieger, T. Schmitt, M. N. Ali, G. Rossi, R. Thomale *et al.*, Phys. Rev. Lett. **119**, 026403 (2017).
[8] A. S. Ngankeu, S. K. Mahatha, K. Guilloy, M. Bianchi, C. E. Sanders, K. Hanff, K. Rossnagel, J. A. Miwa, C. Breth Nielsen, M. Bremholm *et al.*, Phys. Rev. B **96**, 195147 (2017).
[9] M. M. Ugeda, A. J. Bradley, S.-F. Shi, F. H. da Jornada, Y. Zhang, D. Y. Qiu, W. Ruan, S.-K. Mo, Z. Hussain, Z.-X. Shen *et al.*, Nat Mater **13**, 1091 (2014).
[10] D. Y. Qiu, F. H. da Jornada, and S. G. Louie, Phys. Rev. Lett. **111**, 216805 (2013).
[11] A. Grubišić Čabo, J. A. Miwa, S. S. Grønborg, J. M. Riley, J. C. Johannsen, C. Cacho, O. Alexander, R. T. Chapman, E. Springate, M. Grioni *et al.*, Nano Lett. **15**, 5883 (2015).
[12] M. Rösner, C. Steinke, M. Lorke, C. Gies, F. Jahnke, and T. O. Wehling, Nano Lett. **16**, 2322 (2016).
[13] J. A. Galvis, L. Chirolli, I. Guillamón, S. Vieira, E. Navarro-Moratalla, E. Coronado, H. Suderow, and F. Guinea, Phys. Rev. B **89**, 224512 (2014).
[14] E. Navarro-Moratalla, J. O. Island, S. Manas-Valero, E. Pinilla-Cienfuegos, A. Castellanos-Gomez, J. Quereda, G. Rubio-Bollinger, L. Chirolli, J. A. Silva-Guillen, N. Agrait *et al.*, Nat. Commun. **7**, 11043 (2016).
[15] J. Peng, Z. Yu, J. Wu, Y. Zhou, Y. Guo, Z. Li, J. Zhao, C. Wu, and Y. Xie, ACS Nano **12**, 9461 (2018).
[16] X. Xi, L. Zhao, Z. Wang, H. Berger, L. Forró, J. Shan, and K. F. Mak, Nat. Nanotechnol. **10**, 765 (2015).
[17] M. M. Ugeda, A. J. Bradley, Y. Zhang, S. Onishi, Y. Chen, W. Ruan, C. Ojeda-Aristizabal, H. Ryu, M. T. Edmonds, H.-Z. Tsai *et al.*, Nat. Phys. **12**, 92 (2016).
[18] M. Naito and S. Tanaka, J. Phys. Soc. Jpn. **51**, 219 (1982).
[19] I. Guillamón, H. Suderow, S. Vieira, L. Cario, P. Diener, and P. Rodière, Phys. Rev. Lett. **101**, 166407 (2008).
[20] C. Heil, S. Poncé, H. Lambert, M. Schlipf, E. R. Margine, and F. Giustino, Phys. Rev. Lett. **119**, 087003 (2017).
[21] M. Leroux, L. Cario, A. Bosak, and P. Rodière, Phys. Rev. B **97**, 195140 (2018).
[22] A. Kozhakhmetov, T. H. Choudhury, Z. Y. A. Balushi, M. Chubarov, and J. M. Redwing, J. Cryst. Growth **486**, 137 (2018).
[23] H. Bark, Y. Choi, J. Jung, J. H. Kim, H. Kwon, J. Lee, Z. Lee, J. H. Cho, and C. Lee, Nanoscale **10**, 1056 (2018).
[24] A. Kuc, N. Zibouche, and T. Heine, Phys. Rev. B **83**, 245213 (2011).
[25] C. Heil, M. Schlipf, and F. Giustino, Phys. Rev. B **98**, 075120 (2018).
[26] Y. Zhou, Z. Wang, P. Yang, X. Zu, L. Yang, X. Sun, and F. Gao, ACS Nano **6**, 9727 (2012).

[27] F. Güller, V. L. Vildosola, and A. M. Llois, Phys. Rev. B **93**, 094434 (2016).
[28] E. G. C. P. van Loon, M. Rösner, G. Schönhoff, M. I. Katsnelson, and T. O. Wehling, npj Quantum Mater. **3**, 32 (2018).
[29] J. V. Lauritsen, J. Kibsgaard, S. Helveg, H. Topsoe, B. S. Clausen, E. Laegsgaard, and F. Besenbacher, Nat. Nanotechnol. **2**, 53 (2007).
[30] H. Füchtbauer, A. Tuxen, Z. Li, H. Topsøe, J. Lauritsen, and F. Besenbacher, Top. Catal. **57**, 207 (2014).
[31] J. A. Miwa, S. Ulstrup, S. G. Sørensen, M. Dendzik, A. G. Čabo, M. Bianchi, J. V. Lauritsen, and P. Hofmann, Phys. Rev. Lett. **114**, 046802 (2015).
[32] M. Dendzik, M. Michiardi, C. Sanders, M. Bianchi, J. A. Miwa, S. S. Grønborg, J. V. Lauritsen, A. Bruix, B. Hammer, and P. Hofmann, Phys. Rev. B **92**, 245442 (2015).
[33] C. E. Sanders, M. Dendzik, A. S. Ngankeu, A. Eich, A. Bruix, M. Bianchi, J. A. Miwa, B. Hammer, A. A. Khajetoorians, and P. Hofmann, Phys. Rev. B **94**, 081404(R) (2016).
[34] F. Arnold, R.-M. Stan, S. K. Mahatha, H. E. Lund, D. Curcio, M. Dendzik, H. Bana, E. Travaglia, L. Bignardi, P. Lacovig *et al.*, 2D Mater. **5**, 045009 (2018).
[35] J. V. Barth, H. Brune, G. Ertl, and R. J. Behm, Phys. Rev. B **42**, 9307 (1990).
[36] F. Besenbacher, E. Lægsgaard, K. Mortensen, U. Nielsen, and I. Stensgaard, Rev. Sci. Instrum. **59**, 1035 (1988).
[37] I. Horcas, R. Fernández, J. M. Gómez-Rodríguez, J. Colchero, J. Gómez-Herrero, and A. M. Baro, Rev. Sci. Instrum. **78**, 013705 (2007).
[38] S. V. Hoffmann, C. Søndergaard, C. Schultz, Z. Li, and P. Hofmann, Nucl. Instrum. Methods Phys. Res., A **523**, 441 (2004).
[39] S. S. Grønborg, S. Ulstrup, M. Bianchi, M. Dendzik, C. E. Sanders, J. V. Lauritsen, P. Hofmann, and J. A. Miwa, Langmuir **31**, 9700 (2015).
[40] C. Zhang, M.-Y. Li, J. Tersoff, Y. Han, Y. Su, L.-J. Li, D. A. Muller, and C.-K. Shih, Nat. Nanotechnol. **13**, 152 (2018).
[41] H. Bana, E. Travaglia, L. Bignardi, P. Lacovig, C. E. Sanders, M. Dendzik, M. Michiardi, M. Bianchi, D. Lizzit, F. Presel *et al.*, 2D Mater. **5**, 035012 (2018).
[42] S. LaShell, B. A. McDougall, and E. Jensen, Phys. Rev. Lett. **77**, 3419 (1996).
[43] N. Takeuchi, C. T. Chan, and K. M. Ho, Phys. Rev. B **43**, 13899 (1991).
[44] A. Bruix, J. A. Miwa, N. Hauptmann, D. Wegner, S. Ulstrup, S. S. Grønborg, C. E. Sanders, M. Dendzik, A. Grubišić Čabo, M. Bianchi *et al.*, Phys. Rev. B **93**, 165422 (2016).
[45] M. Dendzik, A. Bruix, M. Michiardi, A. S. Ngankeu, M. Bianchi, J. A. Miwa, B. Hammer, P. Hofmann, and C. E. Sanders, Phys. Rev. B **96**, 235440 (2017).
[46] B. Shao, A. Eich, C. Sanders, A. S. Ngankeu, M. Bianchi, P. Hofmann, A. A. Khajetoorians, and T. O. Wehling, Nat. Commun. **10**, 180 (2019).
[47] N. F. Hinsche, A. S. Ngankeu, K. Guilloy, S. K. Mahatha, A. Grubišić Čabo, M. Bianchi, M. Dendzik, C. E. Sanders, J. A. Miwa, H. Bana, E. Travaglia, P. Lacovig, L. Bignardi, R. Larciprete, A. Baraldi, S. Lizzit, K. S. Thygesen, and P. Hofmann, Phys. Rev. B **96**, 121402(R) (2017).
[48] S. K. Mahatha, A. S. Ngankeu, N. F. Hinsche, I. Mertig, K. Guilloy, P. L. Matzen, M. Bianchi, C. E. Sanders, J. A. Miwa, H. Bana *et al.*, Surf. Sci. **681**, 64 (2019).
[49] M. Hengsberger, D. Purdie, P. Segovia, M. Garnier, and Y. Baer, Phys. Rev. Lett. **83**, 592 (1999).
[50] P. Hofmann, I. Y. Sklyadneva, E. D. L. Rienks, and E. V. Chulkov, New J. Phys. **11**, 125005 (2009).
[51] N. Sirica, S.-K. Mo, F. Bondino, I. Pis, S. Nappini, P. Vilmercati, J. Yi, Z. Gai, P. C. Snijders, P. K. Das *et al.*, Phys. Rev. B **94**, 075141 (2016).